

# Primordial magnetic fields from self-ordering scalar fields

Kouichirou Horiguchi,<sup>a,1</sup> Kiyotomo Ichiki,<sup>a,b</sup> Toyokazu Sekiguchi<sup>c</sup>  
and Naoshi Sugiyama<sup>a,b,d</sup>

<sup>a</sup>Department of Physics and Astrophysics, Nagoya University,  
Aichi 464-8602, Japan

<sup>b</sup>Kobayashi-Maskawa Institute for the Origin of Particles and the Universe,  
Nagoya University,  
Nagoya 464-8602, Japan

<sup>c</sup>Helsinki Institute of Physics, University of Helsinki,  
PO Box 64, FIN-00014, Finland

<sup>d</sup>Kavli Institute for the Physics and Mathematics of the Universe (Kavli IPMU), The Uni-  
versity of Tokyo,  
Chiba 277-8582, Japan

E-mail: [horiguchi.kouichirou@h.mbox.nagoya-u.ac.jp](mailto:horiguchi.kouichirou@h.mbox.nagoya-u.ac.jp), [ichiki@a.phys.nagoya-u.ac.jp](mailto:ichiki@a.phys.nagoya-u.ac.jp),  
[toyokazu.sekiguchi@helsinki.fi](mailto:toyokazu.sekiguchi@helsinki.fi), [naoshi@nagoya-u.jp](mailto:naoshi@nagoya-u.jp)

**Abstract.** A symmetry-breaking phase transition in the early universe could have led to the formation of cosmic defects. Because these defects dynamically excite not only scalar and tensor type cosmological perturbations but also vector type ones, they may serve as a source of primordial magnetic fields. In this study, we calculate the time evolution and the spectrum of magnetic fields that are generated by a type of cosmic defects, called global textures, using the non-linear sigma (NLSM) model. Based on the standard cosmological perturbation theory, we show, both analytically and numerically, that a vector-mode relative velocity between photon and baryon fluids is induced by textures, which inevitably leads to the generation of magnetic fields over a wide range of scales. We find that the amplitude of the magnetic fields is given by  $B \sim 10^{-9}((1+z)/10^3)^{-2.5} (v/m_{\text{pl}})^2 (k/\text{Mpc}^{-1})^{3.5} / \sqrt{N}$  Gauss in the radiation dominated era for  $k \lesssim 1 \text{ Mpc}^{-1}$ , with  $v$  being the vacuum expectation value of the O(N) symmetric scalar fields. By extrapolating our numerical result toward smaller scales, we expect that  $B \sim 10^{-17}((1+z)/1000)^{-1/2} (v/m_{\text{pl}})^2 (k/\text{Mpc}^{-1})^{1/2} / \sqrt{N}$  Gauss on scales of  $k \gtrsim 1 \text{ Mpc}^{-1}$  at redshift  $z \gtrsim 1100$ . This might be a seed of the magnetic fields observed on large scales today.

---

<sup>1</sup>Corresponding author.

---

## Contents

<b>1</b>	<b>Introduction</b>	<b>1</b>
<b>2</b>	<b>Non-linear sigma model (NLSM)</b>	<b>3</b>
<b>3</b>	<b>Magnetic fields</b>	<b>4</b>
3.1	Vector mode perturbations and their evolution equations	4
3.1.1	Tight-coupling approximation	6
3.2	Magnetic field generation	7
<b>4</b>	<b>Analytical Understanding</b>	<b>8</b>
4.1	Super-horizon	9
4.2	Sub-horizon	10
4.2.1	case (i) $k \sim q \gg \eta^{-1}$	10
4.2.2	case (ii) $q \ll \eta^{-1}$	10
4.2.3	case (iii) $\eta^{-1} < q < \alpha\eta^{-1}$	10
4.3	Approximation at super-horizon scale	12
4.4	After recombination	12
<b>5</b>	<b>Conclusion</b>	<b>13</b>
<b>A</b>	<b>Appendix</b>	<b>14</b>
A.1	Appendix A : Power spectrum in the NLSM	14

---

## 1 Introduction

The standard big-bang cosmological model has been established by a variety of astronomical observations, such as the dimming of distant supernovae, the cosmic microwave background (CMB), the large-scale structure of the universe, and so on. In this big-bang paradigm, it is naturally expected that the universe experienced a number of phase transitions at the early stages of cosmic history, because of cooling from a very hot initial state caused by its adiabatic expansion. As a result of these phase transitions, topological defects may have been formed and may have acted as a source of large scale structure in the universe. Among others, topological defects resulting from a phase transition that breaks a global  $O(N)$  symmetry are called  $O(N)$  global defects. For example,  $O(N)$  symmetric scalar fields can yield domain walls ( $N = 1$ ), monopoles ( $N = 3$ ), and textures ( $N \geq 4$ ) when the scalar fields break the global symmetry.

There exist many studies regarding the phenomenological aspects of topological defects, which include the generation of CMB temperature and polarization anisotropies [1–4], gravitational waves (GWs)[5–9], and cosmic rays [10, 11], among others (for a review of structure formation with topological defects, see [12]). As a rule of thumb, the amplitude of the fluctuations induced by topological defects, such as CMB anisotropies, is of the order  $\Delta T/T \sim 4\pi Gv^2$ , where  $v$  is the vacuum expectation value (VEV) of the scalar fields,  $G$  is the Newton constant, and  $T$  and  $\Delta T$  are the CMB temperature and its fluctuation, respectively. Therefore, the recent CMB measurement by the Planck satellite has placed limits on the

energy scale of the topological defects [13]. The actual limits depend on the detailed models, for instance,  $Gv^2 \leq 4.2 \times 10^{-7}$  [14] for cosmic strings,  $Gv^2 \leq 3.2 \times 10^{-7}$  for Abelian–Higgs cosmic strings,  $Gv^2 \leq 1.5 \times 10^{-7}$  for Nambu–Goto strings, and  $Gv^2 \leq 1.1 \times 10^{-6}$  for semi-local strings and global textures [13].

In this paper, we pay particular attention to global textures with  $N \gg 4$ , which can be well-approximated by self-ordering scalar fields that follow the non-linear sigma model (NLSM). The NLSM can describe the evolution of global  $O(N)$  symmetric scalar fields with an accuracy up to corrections on the order of  $1/N$ . The NLSM has attracted much attention since the discovery of CMB B-mode polarizations by the BICEP2 experiment [15] because textures following the NLSM can be a source of the scale-invariant GWs [16][7][5], just as inflation in the early universe can produce the scale-invariant GWs. To observationally distinguish between GWs originating from inflation and from textures, one should consider observables that reflect the time evolution of the GWs. The GWs from inflation are frozen on super-horizon scales at first, and decay with oscillations after the horizon crossing. The GWs from textures, on the other hand, are generated inside the horizon, and decay with oscillations after the scalar fields that source the GWs decay away as the universe expands. In [17], the authors calculate the CMB temperature and polarization anisotropies in the NLSM and find that the shapes of the correlation functions of the CMB anisotropies in the NLSM are different from the corresponding ones from inflation. Therefore, detailed observations of CMB anisotropies can distinguish between GWs from the two different origins. In fact, the recent B-mode measurement by BICEP2 places an upper bound on the VEV in the NLSM at  $v \lesssim 9 \times 10^{-4} G^{-1/2}$ , and the GWs from the NLSM are shown to be slightly disfavored by the data compared with those from inflation [18][19], while contamination by dust in the BICEP2 data has to be re-analyzed with PLANCK data.

In this paper, we investigate yet another route to probe the NLSM: the generation of magnetic fields. Because of the non-linear nature of the NLSM, scalar fields following the NLSM inevitably induce vector-mode perturbations as well as scalar and tensor-mode ones. The relative vector-mode velocity between photon and baryon fluids induces rotation in electric fields, leading to the generation of magnetic fields [20]. Recent discoveries of large-scale magnetic fields in void regions [21][22] as well as magnetic fields at high redshifts [23] make the investigation more interesting because such magnetic fields may be of primordial origin in the early universe. Therefore, one of the aims of this paper is to derive the spectrum of magnetic fields generated by vector perturbations in the NLSM within the observational limits of CMB anisotropies.

This paper is organized as follows. In the next section, we review the NLSM, in which  $N$ -component scalar fields act as a source of cosmological perturbations. In section 3, we derive the power spectrum of magnetic fields in the NLSM, both numerically and analytically, using the tight coupling approximation. We will see that in order to obtain a reliable result, we should expand the equations up to the third order in the tight coupling approximation between photon and baryon fluids. We discuss the result and give an analytic interpretation of the spectrum of the magnetic fields in section 4, followed by our conclusion in section 5. Throughout this paper, we fix the cosmological parameters to  $h = 0.7$ ,  $\Omega_b h^2 = 0.0226$ ,  $\Omega_c h^2 = 0.112$ , and  $N_\nu = 3.046$ , where  $H_0 = 100h$  km/s/Mpc is the Hubble constant,  $\Omega_b$  and  $\Omega_c$  are the density parameters of baryonic and cold dark matter, respectively, and  $N_\nu$  is the effective number of massless neutrinos. Those parameter values are consistent with the Planck results, and correspond to the  $\Lambda$ CDM model [24].

## 2 Non-linear sigma model (NLSM)

We consider a model of  $N$  scalar fields with a global  $O(N)$  symmetry, which undergoes symmetry breaking in the early universe. The Lagrangian of the model is given by

$$\mathcal{L} = -\frac{1}{2}\nabla_\mu\Phi^t\nabla^\mu\Phi - \frac{\lambda}{4}(\Phi^t\Phi - v^2)^2 + \mathcal{L}_T. \quad (2.1)$$

Here  $\Phi = (\phi_1, \phi_2, \dots, \phi_N)$  is an array of  $N$  real scalar fields,  $v$  is the vacuum expectation value (VEV) of the scalar fields after symmetry breaking,  $\lambda$  is the self-coupling constant, and  $\mathcal{L}_T \sim T^2\Phi^t\Phi$  is the thermal term of the Lagrangian. Deep in the radiation-dominated universe, the thermal term is dominant in the Lagrangian of the scalar fields. As the temperature of the universe goes down, this thermal term gets smaller. When the term becomes negligible a spontaneous symmetry breaking occurs. At energy scales well below  $v$ , the field values are confined on the  $N - 1$  dimensional sphere in the  $N$  dimensional field space so that  $\Phi^t(\vec{x}, \eta)\Phi(\vec{x}, \eta) = v^2$ . Under this condition, in the large- $N$  limit, the equation of motion for the scalar fields can be derived as

$$\nabla^\mu\nabla_\mu\beta_a + (\nabla_\mu\beta_b) \cdot (\nabla^\mu\beta_b)\beta_a = 0, \quad (2.2)$$

where the indices  $a$  and  $b$  run over  $1, \dots, N$  and summations with respect to deprecated indices are implicit. This is the equation of motion for the scalar fields in the NLSM. If  $N \leq 3$ , topological defects such as domain walls, cosmic strings and monopoles are produced, where the scalar fields can restore the  $O(N)$  symmetry and possess the higher energy density.

In this paper we consider cases with  $N \geq 4$ , where non-topological defects, or textures, form. Let us consider the flat Friedmann-Lemaître-Robertson-Walker universe with the metric

$$ds^2 = g_{\mu\nu}dx^\mu dx^\nu = a^2(\eta)(-d\eta^2 + d\vec{x}^2), \quad (2.3)$$

where  $a(\eta)$  is the cosmic scale factor and  $\eta$  is the conformal time. In the large- $N$  limit, making an ansatz that  $\langle (\nabla_\mu\beta_a) \cdot (\nabla^\mu\beta_a) \rangle = T_0 a^{-2}\eta^{-2}$ , we can obtain the analytic solution as [7] [5]

$$\beta_a(\vec{k}, \eta) = \sqrt{A_\nu} \left( \frac{\eta}{\eta_*} \right)^{3/2} \frac{J_\nu(k\eta)}{(k\eta)^\nu} \beta_a(\vec{k}, \eta_*) \equiv f(k, \eta, \eta_*)\beta_a(\vec{k}, \eta_*), \quad (2.4)$$

where  $\nu = d \ln a / d \ln \eta + 1$ ,  $A_\nu = 4\Gamma(2\nu - 1/2)\Gamma(\nu - 1/2)/3\Gamma(\nu - 1)$  and  $T_0 = 3\nu - 9/4$ . In eq. (2.4),  $\eta_*$  is the time of phase transition and  $\beta_a(\vec{k}, \eta_*)$  is the initial value of scalar fields, whose two-point correlation function can be given as

$$\langle \beta_a(\vec{k}_1, \eta_*)\beta_b^*(\vec{k}_2, \eta_*) \rangle = \frac{6\pi^2\eta_*^3}{N}\delta_{ab} (2\pi)^3\delta(\vec{k}_1 - \vec{k}_2). \quad (2.5)$$

The above relation is only valid for  $k \ll 1/\eta_*$ , which follows, in the large- $N$  limit, from the fact that the scalar fields take their VEV independently in each horizon at  $\eta_*$ .<sup>1</sup> We also note that  $\beta_a(\vec{k}, \eta_*)$  is Gaussian at these scales.

We denote a correlation function of  $\beta_a$  as a product of the transfer function and the initial amplitude as

$$\langle \beta_a(\vec{k}_1, \eta)\beta_b^*(\vec{k}_2, \eta) \rangle = F(k_1, k_2, \eta, \eta_*) \langle \beta_a(\vec{k}_1, \eta_*)\beta_b^*(\vec{k}_2, \eta_*) \rangle, \quad (2.6)$$

---

<sup>1</sup> On small scales  $k \gtrsim 1/\eta_*$ , initial scalar fields become homogenous and correlation function of eq. (2.5) should vanish. We however note that our argument does not depend on the correlation function on these scales.

where  $F(k_1, k_2, \eta, \eta_*) \equiv f(k_1, \eta, \eta_*)f(k_2, \eta, \eta_*)$ . From eq.(2.4) and eq.(2.5), we can see that the dependence of eq.(2.6) on  $\eta_*$  is canceled out. Therefore we omit  $\eta_*$  from the equations hereafter and write as  $F(k_1, k_2, \eta, \eta_*) = F(k_1, k_2, \eta)$  and  $\beta_a(\vec{k}, \eta_*) = \beta_a(\vec{k})$ . Finally the energy-momentum tensor of the scalar fields is given by

$$T_{\mu\nu}^\phi = v^2 \left[ \partial_\mu \beta_a \partial_\nu \beta_a - \frac{1}{2} g_{\mu\nu} \partial_\lambda \beta_a \partial^\lambda \beta_a \right]. \quad (2.7)$$

### 3 Magnetic fields

In this section, we investigate generation of seeds of large scale magnetic fields from the self-ordering scalar fields which follow the NLSM. These scalar fields can induce cosmological vector-mode perturbations and eventually produce magnetic fields.

#### 3.1 Vector mode perturbations and their evolution equations

We begin by reviewing the basic linear perturbation theory and define the vector mode. Let us consider the perturbed metric around the flat FRW one in the synchronous gauge as

$$ds^2 = g_{\mu\nu} dx^\mu dx^\nu = a^2(\eta) (-d\eta^2 + (\delta_{ij} + h_{ij}) dx^i dx^j), \quad (3.1)$$

where  $h_{ij}$  is the metric perturbation. In Fourier space, the vector part of  $h_{ij}$  can be expressed as

$$h_{ij} = \frac{i\hat{k}_i h_j^V + i\hat{k}_j h_i^V}{\sqrt{2}}. \quad (3.2)$$

Here  $h_i^V$  is a divergenceless vector and can be rewritten using the vector basis  $e_i^{(\pm)}(\hat{k})$  as

$$h_i^V = \sum_{\lambda=\pm} \lambda h_V^{(\lambda)} e_i^{(\lambda)}(\hat{k}). \quad (3.3)$$

Combining eq. (3.2) and eq. (3.3), we can denote  $h_{ij}$  directly as

$$h_{ij} = \sum_{\lambda=\pm} h_V^{(\lambda)} \mathcal{O}_{ij}^{(\lambda)}, \quad \mathcal{O}_{ij}^{(\lambda)} = \frac{i\lambda}{\sqrt{2}} (\hat{k}_i e_j^{(\lambda)}(\hat{k}) + \hat{k}_j e_i^{(\lambda)}(\hat{k})), \quad (3.4)$$

where  $\mathcal{O}_{ij}^{(\lambda)}$  is the vector projection tensor. Using this projection tensor, we can derive the vector-mode perturbation equation for  $\sigma = \dot{h}_V/k$  as

$$\dot{\sigma}^{(\lambda)} + 2\mathcal{H}\sigma^{(\lambda)} = 8\pi G a^2 \Pi^{(\lambda)}/k, \quad (3.5)$$

where  $\Pi^{(\lambda)} = T_{ij}^{(\text{tot})} \mathcal{O}_{ij}^{(\lambda)}$  is the total anisotropic stress in the vector mode,  $\mathcal{H} = \dot{a}/a$  is conformal hubble, and a dot denotes a conformal time derivative. Hereafter we shall omit the superscript  $(\lambda)$  for the purpose of presentation. The total energy-momentum tensor consists of two parts: one is from the ordinary matter and radiation and the other is from the scalar fields given by eq. (2.7). Anisotropic stress of the scalar fields  $\Pi^\phi = T_{ij}^\phi \mathcal{O}_{ij}$  can be calculated as

$$a^2 \Pi^\phi(\vec{k}, \eta) = \frac{v^2}{2} \int \frac{d^3 p}{(2\pi)^3} \frac{d^3 q}{(2\pi)^3} \sqrt{1 - \mu^2} [k - 2q\mu] q F(q, p, \eta) \beta_a(\vec{p}) \beta_a(\vec{q}) (2\pi)^3 \delta(\vec{k} - \vec{p} - \vec{q}), \quad (3.6)$$

where  $\mu = \hat{k} \cdot \hat{q}$  and  $p = \sqrt{k^2 - 2kq\mu + q^2}$ . For the expression of anisotropic stress of ordinary matter and radiation, we refer to, e.g., ref. [25]. Let us define the transfer function for the anisotropic stress of the scalar fields as

$$a^2 \pi^\phi(k, q, \mu, \eta) \equiv \frac{v^2}{2} \sqrt{1 - \mu^2} [k - 2q\mu] q F(q, p, \eta), \quad (3.7)$$

and the transfer function for  $\sigma$  as

$$\sigma(k, q, \mu, \eta) = \frac{4\pi}{a^2(\eta)} \frac{v^2}{m_{\text{pl}}^2} \int^\eta d\eta' a^2(\eta') \sqrt{1 - \mu^2} [k - 2q\mu] q F(q, p, \eta')/k. \quad (3.8)$$

The fluid equation for baryon in the vector mode is given by

$$\dot{v}_b + \mathcal{H}v_b = \frac{4\rho_\gamma}{3\rho_b} an_e \sigma_T (v_\gamma - v_b), \quad (3.9)$$

where  $\rho_\gamma$  and  $\rho_b$  are the energy densities of photon and baryon fluids, respectively,  $R = 4\rho_\gamma/3\rho_b$ ,  $\sigma_T$  is the Thomson scattering cross section,  $n_e$  is the electron number density, and  $an_e \sigma_T = \dot{\tau}$  is the opacity of the Thomson scattering. On the other hand, the vector-mode Boltzmann equation of photon fluid expanded in terms of multipole momenta is given by

$$\dot{v}_\gamma + \frac{1}{8}k\Pi_\gamma = -\dot{\tau}(v_\gamma - v_b), \quad (3.10)$$

$$\dot{\Pi}_\gamma + \frac{8}{5}kI_3 - \frac{8}{5}kv_\gamma = -\dot{\tau} \left( \frac{9}{10}\Pi_\gamma - \frac{9}{5}E_2 \right) + \frac{8}{5}k\sigma, \quad (3.11)$$

$$\dot{I}_l + k \frac{l}{2l+1} \left( \frac{l+2}{l+1} I_{l+1} - I_{l-1} \right) = -\dot{\tau} I_l \quad (\text{for } l \geq 3), \quad (3.12)$$

for intensity and

$$\dot{E}_l + \frac{(l+3)(l+2)l(l-1)}{(l+1)^3(2l+1)} kE_{l+1} - \frac{l}{2l+1} kE_{l-1} = -\dot{\tau} \left( E_l - \frac{2}{15}\zeta\delta_{l2} \right) + \frac{2}{l(l+1)} kB_l, \quad (3.13)$$

$$\dot{B}_l + \frac{(l+3)(l+2)l(l-1)}{(l+1)^3(2l+1)} kB_{l+1} - \frac{l}{2l+1} kB_{l-1} = -\frac{2}{l(l+1)} kE_l, \quad (3.14)$$

for polarization. Here  $v_\gamma$  and  $\Pi_\gamma$  are the velocity and anisotropic stress of photons, respectively,  $I_l$  is the  $l$ -th order moment of photons' distribution, and  $E_l$  and  $B_l$  are the photons' polarization moments and  $\zeta \equiv 3I_2/4 + 9E_2/2$  [26].

As we shall show in section 3.2, the relative velocity between the photon and baryon fluids plays the key role in generation of magnetic fields. Since the strength of the coupling between photon and baryon velocities significantly changes before and after recombination, evolution of the relative velocity and hence the magnetic fields qualitatively differs between these two epochs. Before recombination, the tight-coupling approximation allows us to solve the system of equations partially, which we shall see shortly, and helps us to interpret numerical results. On the other hand, after recombination, the system of equations is solved completely numerically.

### 3.1.1 Tight-coupling approximation

In the early universe, photon and baryon fluids are tightly coupled because the opacity of the Thomson scattering  $\dot{\tau}$  is very large. Therefore we can expand the perturbation equations in section 3.1 in terms of the tight-coupling parameter  $k/\dot{\tau} \ll 1$ . This is called the tight coupling approximation (TCA). In ordinary analyses without external sources such as the NLSM, the first order solution for anisotropic stress of photons  $\Pi_g^{(1)}$  and the second order solution for the relative velocity between the photon and baryon fluids  $\delta v^{(2)} = v_\gamma^{(2)} - v_b^{(2)}$  were used [20]. However, when there exist NLSM scalar fields as an external source in the linearized Boltzmann system, we find that one should consider the TCA up to the third order terms proportional to  $\sigma$ , as discussed below.

In the tight coupling expansion, the baryon velocity relative to the photon velocity is expanded using the tight coupling parameter, i.e.,  $v_\gamma - v_b = 0 + \delta v^{(1)} + \delta v^{(2)} + \dots$ , where  $\delta v^{(1)}$  and  $\delta v^{(2)}$  are proportional to  $(k/\dot{\tau})$  and  $(k/\dot{\tau})^2$ , respectively. The tight coupling solutions of  $\Pi_\gamma$  and  $\delta v$  up to the second order are given by

$$\begin{aligned}\Pi_\gamma^{(1)} &= \frac{32}{15} \left(\frac{k}{\dot{\tau}}\right) (v_\gamma^{(0)} + \sigma^{(0)}), \\ \Pi_\gamma^{(2)} &= \frac{32}{15} \left(\frac{k}{\dot{\tau}}\right) (v_\gamma^{(1)} + \sigma^{(1)}) + \frac{176}{45} \left(\frac{k}{\dot{\tau}}\right)^2 \frac{1}{k} \left[ \frac{\ddot{\tau}}{\dot{\tau}} (v_\gamma^{(0)} + \sigma^{(0)}) - (\dot{v}_\gamma^{(0)} + \dot{\sigma}^{(0)}) \right]\end{aligned}\quad (3.15)$$

$$\delta v^{(1)} = \left(\frac{k}{\dot{\tau}}\right) \frac{\mathcal{H}}{(1+R)k} v_\gamma^{(0)} \quad (3.16)$$

$$\begin{aligned}\delta v^{(2)} &= \left(\frac{k}{\dot{\tau}}\right) \frac{\mathcal{H}}{(1+R)k} v_\gamma^{(1)} - \frac{4}{15} \left(\frac{k}{\dot{\tau}}\right)^2 \frac{1}{1+R} (v_\gamma^{(0)} + \sigma^{(0)}) \\ &\quad - \left(\frac{k}{\dot{\tau}}\right)^2 \frac{\mathcal{H}v_\gamma^{(0)}}{(1+R)^2 k^2} \left( \frac{\mathcal{H}R}{1+R} + \frac{\dot{\mathcal{H}}}{\mathcal{H}} + \mathcal{H} + \frac{\dot{v}_\gamma^{(0)}}{v_\gamma^{(0)}} - \frac{\ddot{\tau}}{\dot{\tau}} \right)\end{aligned}\quad (3.17)$$

It is important to note that  $\delta v^{(2)}$  is not necessarily smaller than  $\delta v^{(1)}$  in the NLSM. This is because, in the NLSM, the metric perturbation  $\sigma$  is always much larger than the fluid perturbation variables such as  $v_\gamma$  (see figure 1 and discussion in section 4), and it sometimes happens that the first order solution proportional to  $v_\gamma$  is smaller than the second order solution proportional to  $\sigma$  i.e.  $(k/\dot{\tau})v_\gamma \lesssim (k/\dot{\tau})^2\sigma$ . We can see directly this relation from (3.10), which implies

$$v_\gamma \sim k \int d\eta \frac{k}{\dot{\tau}} \sigma \sim k\eta \left(\frac{k}{\dot{\tau}}\right) \sigma. \quad (3.18)$$

Therefore, the condition that  $(k/\dot{\tau})v_\gamma \lesssim (k/\dot{\tau})^2\sigma$  is satisfied at least on super-horizon scales, and the slip term is dominated by the second order terms in the tight coupling approximation.

In fact, in the numerical calculations, we must eventually switch to evaluate the slip term directly from  $v_\gamma$  and  $v_b$  because the tight coupling approximation breaks down in late times. Because the slip term is dominated by the second order term  $\delta v^{(2)}$  in early times, we must keep solving  $v_\gamma$  and  $v_b$  accurate enough up to the second order in the tight coupling approximation, i.e.,  $v_\gamma^{(2)}$  and  $v_b^{(2)}$ . In terms of the tight coupling approximation, the evolution equation of  $v_\gamma^{(2)}$ , for instance, is given by

$$\dot{v}_\gamma^{(2)} = -\frac{1}{8} k \Pi_\gamma^{(2)} - \dot{\tau} \delta v^{(3)}. \quad (3.19)$$

This is why we need to consider TCA up to the third order. The slip term at the third order is given by

$$\begin{aligned}
\delta v^{(3)} = & \left(\frac{k}{\dot{\tau}}\right) \frac{\mathcal{H}}{(1+R)k} v_\gamma^{(2)} - \frac{4}{15} \left(\frac{k}{\dot{\tau}}\right)^2 \frac{1}{1+R} (v_\gamma^{(1)} + \sigma^{(1)}) \\
& - \left(\frac{k}{\dot{\tau}}\right)^2 \frac{\mathcal{H} v_\gamma^{(1)}}{(1+R)^2 k^2} \left( \frac{\mathcal{H} R}{1+R} + \frac{\dot{\mathcal{H}}}{\mathcal{H}} + \mathcal{H} + \frac{\dot{v}_\gamma^{(1)}}{v_\gamma^{(1)}} - \frac{\dot{\tau}}{\tau} \right) \\
& + \frac{4}{15} \left(\frac{k}{\dot{\tau}}\right)^3 \frac{\mathcal{H}}{(1+R)^2 k} \sigma^{(0)} \\
& - \frac{2}{45k} \left(\frac{k}{\dot{\tau}}\right)^3 \frac{1}{(1+R)^2} \left[ (23+11R) \frac{\ddot{\tau}}{\dot{\tau}} \sigma^{(0)} - (17+11R) \dot{\sigma}^{(0)} - \frac{6\sigma^{(0)} \mathcal{H} R}{1+R} \right]. \quad (3.20)
\end{aligned}$$

Here we show only the terms proportional to  $\sigma$ . The condition  $\delta v^{(3)} \ll \delta v^{(2)}$  is always valid in the tight coupling regime.

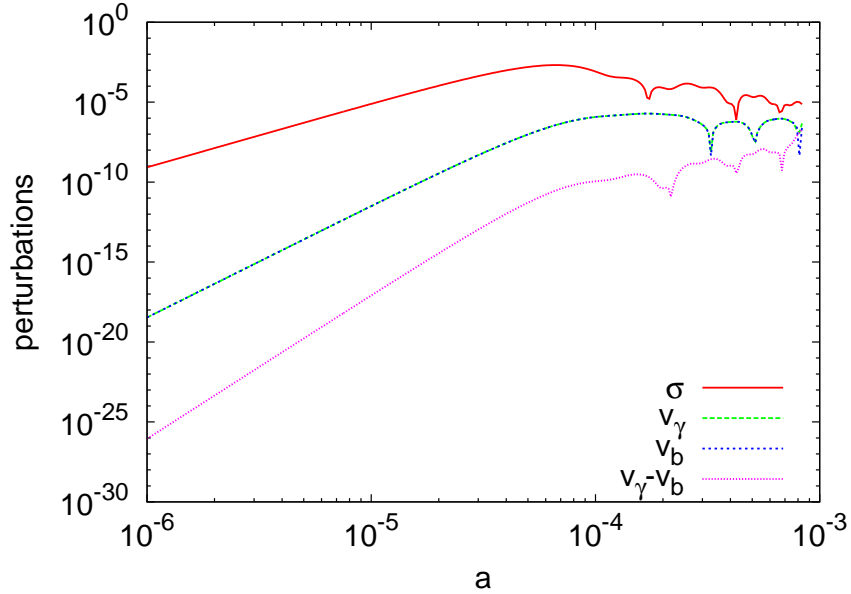


**Figure 1.** Time-evolutions of the transfer functions. Here  $\sigma(k, q, \mu, \eta)$  (red line),  $v_\gamma(k, q, \mu, \eta)$  (green),  $v_b(k, q, \mu, \eta)$  (blue) and  $\delta v(k, q, \mu, \eta)$  (magenta) are plotted as functions of the scale factor. We assume  $k = q = 10^{-1} \text{Mpc}^{-1}$  and,  $\mu = 0$ . We can see that the condition  $\sigma \gg v_\gamma$  is almost always satisfied.

### 3.2 Magnetic field generation

We consider generation of magnetic fields originated from the relative velocity between the photon and baryon fluids,  $\delta v = v_\gamma - v_b$ . Well before recombination, due to the frequent Thomson scattering of photons off electrons, electrons are separated with protons, and move together with photons. For protons to catch up with electrons, electric fields are induced and rotation of the induced electric fields generates magnetic fields via Maxwell equations.

The equation for the generation of magnetic fields is given by [27]

$$\frac{1}{a} \frac{d}{d\eta} (a^2 B^i) = \frac{4\sigma_T \rho_\gamma a}{3e} \epsilon^{ijk} \partial_k (v_{\gamma j} - v_{b j}), \quad (3.22)$$



where  $e$  is the elementary charge and  $\epsilon^{ijk}$  is the Levi-Civita tensor. The appearance of the rotation of  $\delta v$  in eq. (3.22) clearly shows that only the vector-mode part of  $\delta v$  can contribute to magnetic fields. By integrating eq. (3.22) in Fourier space, we obtain

$$a^4 B^i(\vec{k}, \eta) B_i^*(\vec{k}', \eta) = \left(\frac{4\sigma_T}{3e}\right)^2 (\delta^{jl}\delta^{km} - \delta^{jm}\delta^{kl}) k_k k'_m \int_0^\eta d\eta' a^2(\eta') \rho_\gamma(\eta') \delta v_j(\vec{k}, \eta') \\ \times \int_0^\eta d\eta'' a^2(\eta'') \rho_\gamma(\eta'') \delta v_i^*(\vec{k}', \eta''). \quad (3.23)$$

Next we take an ensemble average of this expression over the initial configuration of the NLSM scalar fields  $\beta_a(\vec{k})$ . The ensemble average of the relative velocity can be calculated using the transfer function  $\delta v(k, q, \mu, \eta)$  and the NLSM's initial power spectrum  $\mathcal{P}_{\text{ini}}^N$  defined in appendix A.1 as

$$\langle \delta v_j(\vec{k}, \eta') \delta v_i^*(\vec{k}', \eta'') \rangle = P_{jl}(\hat{k}) \frac{\mathcal{P}_{\text{ini}}^N}{2\pi^2} (2\pi)^3 \delta(\vec{k} - \vec{k}') \\ \times \int dq q^2 \int d\mu \delta v(k, q, \mu, \eta') \delta v(k, q, \mu, \eta''), \quad (3.24)$$

$$P_{jl}(\hat{k}) = \delta_{jl} - \hat{k}_j \hat{k}_l. \quad (3.25)$$

The correlation function of magnetic fields is then obtained as

$$\langle B^i(\vec{k}, \eta) B_i^*(\vec{k}', \eta) \rangle = (2\pi)^3 S_B(k, \eta) \delta(\vec{k} - \vec{k}'), \quad (3.26)$$

where

$$a^4(\eta) \frac{k^3}{2\pi^2} S_B(k, \eta) = \frac{k^3}{2\pi^2} \left(\frac{4\sigma_T}{3e}\right)^2 \frac{\mathcal{P}_{\text{ini}}^N}{\pi^2} k^2 \int dq q^2 \int_{-1}^1 d\mu \left[ \int_0^\eta d\eta' a^2(\eta') \rho_\gamma(\eta') \delta v(k, q, \mu, \eta') \right]^2. \quad (3.27)$$

We calculate eq. (3.27) numerically and the power spectra of magnetic fields at several redshifts are depicted in figure 2.

## 4 Analytical Understanding

Let us try to understand the results obtained in the previous section analytically. In our numerical calculations, we consider scalar fields following the NLSM as the only source of vector mode cosmological perturbations. Therefore we assume that there are no vector mode perturbations at  $\eta \rightarrow 0$ . In this setup, vorticity  $\sigma$  evolves first with the scalar fields as an external source (eq. (3.6)), and it induces photons' anisotropic stress  $\Pi_\gamma$ . Then  $\Pi_\gamma$  leads to the photon velocity  $v_\gamma$  and it propagates to the baryon velocity  $v_b$ . Because the induced anisotropic stress  $\Pi_\gamma$  is suppressed by a factor of the tight coupling parameter  $k/\dot{\tau}$  due to the frequent Thomson scattering (see eq. (3.15)), the velocities induced from the anisotropic stress are much smaller than  $\sigma$ , in other words, the condition that  $\sigma \gg v_\gamma \sim v_b$  is valid at least in the tight coupling era. Therefore, we can find that the dominant term in eq. (3.17) is

$$\delta v(k, q, \mu, \eta) \approx -\frac{4}{15} \left(\frac{k}{\dot{\tau}}\right)^2 \frac{1}{1+R} \sigma(k, q, \mu, \eta). \quad (4.1)$$

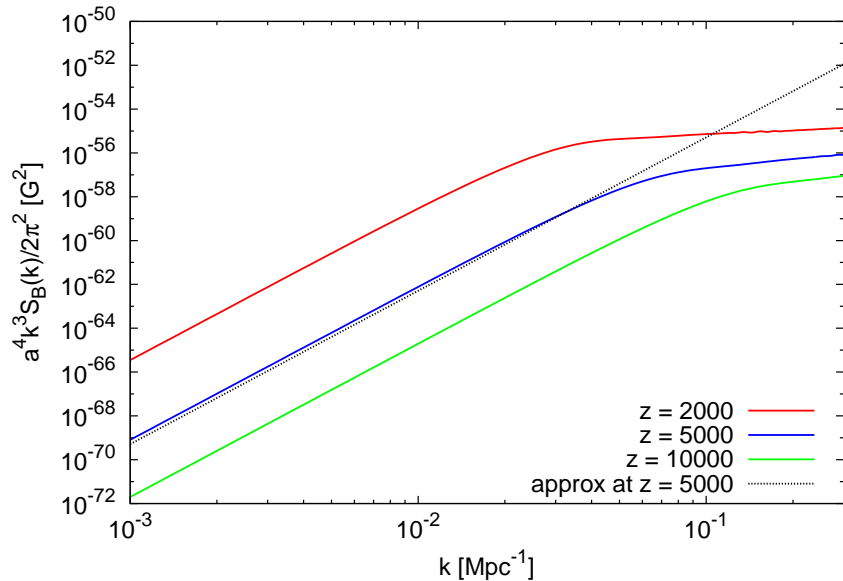


**Figure 2.** Power spectra of magnetic fields at  $z = 2000$  (red solid line),  $z = 5000$  (blue solid line) and  $z = 10000$  (green solid line) from scalar fields in the NLSM. Here we take the NLSM parameters as  $v^4/N = 10^{-12} m_{\text{pl}}^4$ . The black dotted line is the approximate amplitude which is given by eq. (4.18).

To calculate  $\sigma(k, q, \mu, \eta)$ , we introduce approximations for the Bessel function in eq. (2.4) which are given by

$$\frac{J_\nu(x)}{x^\nu} \approx \begin{cases} \frac{1}{2^\nu \Gamma(\nu+1)} & (\text{for } x \ll 1) \\ \frac{1}{x^\nu} \sqrt{\frac{2}{\pi x}} \cos\left(x - \frac{2\nu+1}{4}\pi\right) & (\text{for } x \gg 1) \end{cases}. \quad (4.2)$$

Using these approximations, we can calculate super-horizon ( $k\eta \ll 1$ ) and sub-horizon ( $k\eta \gg 1$ ) solutions in the radiation and matter dominated eras as we shall show below.

#### 4.1 Super-horizon

On super-horizon scales, the wavenumber of fluctuations  $k$  is smaller than the inverse of the horizon scale, i.e.,  $k\eta \ll 1$ . However the wavenumber  $q$  in eq. (3.27) which comes from the convolution integral does not necessarily satisfy  $q\eta \ll 1$ . We know from eq. (3.7) and eq. (4.2) that  $\sigma(k, q, \mu, \eta)$  as a function of  $q$  decays as  $\sigma \propto q^{-2\nu+1}$  for  $q \gg \eta^{-1}$ , and we could expect that the bulk of the  $q$ -integration comes from the range of  $q \lesssim \eta^{-1}$ . In this case we can express eq. (3.27) as

$$a^4 \frac{k^3}{2\pi^2} S_B(k) \propto k^5 \eta^{-3} \left[ \eta a^{-2} \delta v(k, q = 1/\eta, \mu, \eta) \right]^2. \quad (4.3)$$

For  $k \ll q \sim p \sim 1/\eta$ , we can find the  $k$ -dependence of  $\sigma$  from eq. (3.8) as,

$$\sigma \propto \frac{\eta^2}{k}. \quad (4.4)$$

Then, substituting eq. (4.1) and eq. (4.4) into eq. (4.3), we obtain

$$a^4 \frac{k^3}{2\pi^2} S_B(k) \propto k^5 \left[ \frac{k^2}{k} \right]^2 \propto k^7. \quad (4.5)$$

We can see this power law tail on large scales in figure 2. The spectral index is same as that of the magnetic fields generated from second order density perturbations [27], but slightly different from the one obtained in the Einstein-aether gravity model, where  $\sqrt{\langle B_{EA}^2(k) \rangle} \propto k^4$  [28].

## 4.2 Sub-horizon

On sub-horizon scales, i.e.  $k\eta \gg 1$ , the situation changes in a more complicated way. Because of the condition that  $p\eta = \sqrt{k^2 - 2kq\mu + q^2}\eta \gg 1$ , we must take special care of rapid oscillations of the Bessel functions in eqs.(3.8) and (3.27). In order to manipulate the equations analytically, we divide the interval of integration with wavenumber  $q$  into three regions: (i)  $k \sim q \gg \eta^{-1}$ ;  $q$  is on sub-horizon scale, (ii)  $q \ll \eta^{-1}$ ;  $q$  is on super-horizon scale, and (iii)  $\eta^{-1} < q < \alpha\eta^{-1}$ ;  $q$  is nearly on the horizon scale (with  $\alpha$  being  $\mathcal{O}(1)$  constant). Considering contributions from each interval, we estimate the power spectrum of magnetic fields.

### 4.2.1 case (i) $k \sim q \gg \eta^{-1}$

In this case, because the conditions that  $p\eta \gg 1$  and  $q\eta \gg 1$  are satisfied from the conservation of the momentum, the source function of the vorticity  $\sigma$  has decayed away. Without sources, the vorticity also decays and therefore the contribution from this part is negligible.

### 4.2.2 case (ii) $q \ll \eta^{-1}$

In this case,  $p \sim k$  and the source of the vorticity is growing. Using the approximation of eq. (4.2), and assuming the radiation dominated era ( $\nu = 2$ ), we can evaluate eq. (3.8) as

$$\begin{aligned} \sigma &\propto \frac{1}{a^2} \int_0^{\eta'} d\eta'' \eta''^5 q (1 - 2q\mu/k) \frac{J_\nu(k\eta'')}{(k\eta'')^\nu}, \\ &\propto \eta'^{-2} k^{-6} q (k\eta')^3 J_3(k\eta'). \end{aligned} \quad (4.6)$$

Here we use the fact that  $1 - 2q\mu/k \simeq 1$  and the formula  $\int dx x^{n+1} J_n(x) = x^{n+1} J_{n+1}(x)$ , and ignore the factor  $\sqrt{1 - \mu^2}$ . Using the above formula again and eq. (4.1), we obtain

$$\int_0^\eta d\eta' \rho_\gamma a^2 \delta v \propto k^{-6} q (k\eta)^4 J_4(k\eta). \quad (4.7)$$

Substituting eq. (4.7) into eq. (3.27) and using eq. (4.2), the spectrum can be written as

$$\begin{aligned} a^4 \frac{k^3}{2\pi^2} S_B(k) &\propto k^5 \int_0^{1/\eta} dq q^4 [k^{-6} (k\eta)^4 J_4(k\eta)]^2 \\ &\propto k^0. \end{aligned} \quad (4.8)$$

### 4.2.3 case (iii) $\eta^{-1} < q < \alpha\eta^{-1}$

In this range, we need to treat the source carefully. First, assuming the radiation dominated era, let us divide the  $\eta'$  integral in eq. (3.27) as

$$\int_0^\eta a^2(\eta') \rho_\gamma(\eta') \delta v d\eta' \propto \int_0^\eta \eta' \sigma(\eta') d\eta' = \int_0^{q^{-1}} \eta' \sigma_{\eta' < q^{-1}}(\eta') d\eta' + \int_{q^{-1}}^\eta \eta' \sigma_{\eta' > q^{-1}}(\eta') d\eta'. \quad (4.9)$$

The integrand of the first term in the above equation,  $\sigma_{\eta' < q^{-1}}(\eta')$ , is given by eq. (4.6), and the integration leads to the term proportional to  $k^{-6}q(k/q)^4 J_4(k/q)$ . That of the second term is calculated as

$$\begin{aligned}\sigma_{\eta' > q^{-1}}(\eta') &\simeq \frac{1}{a^2} \int_0^{q^{-1}} d\eta'' \eta''^5 q(1 - 2q\mu/k) \frac{J_\nu(k\eta'')}{(k\eta'')^\nu} \\ &+ \frac{1}{a^2} \int_{q^{-1}}^{\eta'} d\eta'' \eta''^5 q(1 - 2q\mu/k) \frac{J_\nu(k\eta'')}{(k\eta'')^\nu} \frac{J_\nu(q\eta'')}{(q\eta'')^\nu} \\ &\propto \eta'^{-2} k^{-6} [q(k/q)^3 J_3(k/q) + k^2 q^{-1} (k\eta') (J_3(k\eta') J_2(q\eta') + \mathcal{O}(q/k))] \quad (4.10)\end{aligned}$$

where we used  $J_\nu(q\eta'')/(q\eta'')^\nu \simeq \mathcal{O}(1)$  for  $q\eta'' \ll 1$ , and omitted the constant factor of  $\mathcal{O}(1)$ .

Then the integration of  $\delta v$  can be calculated, by integrating by parts, as

$$\begin{aligned}\int_0^\eta d\eta' \rho_\gamma a^2 \delta v &\propto [k^{-6} q(k/q)^4 J_4(k/q) + k^{-4} q(k/q)^3 J_3(k/q) (\eta^2 - q^{-2}) \\ &+ k^{-4} q^{-1} (k\eta)^2 J_4(k\eta) J_2(q\eta)]. \quad (4.11)\end{aligned}$$

Substituting the above equation into eq.(3.27) and ignoring the cross terms, we obtain,

$$\begin{aligned}a^4 \frac{k^3}{2\pi^2} S_B(k) &\propto k^5 \int_{1/\eta}^{\alpha/\eta} dq q^2 [k^{-12} q^2 (k/q)^8 J_4^2(k/q) \\ &+ k^{-8} q^2 (k/q)^6 J_3^2(k/q) (\eta^2 - q^{-2})^2 + k^{-8} q^{-2} (k\eta)^4 J_4^2(k\eta) J_2^2(q\eta)]. \quad (4.12)\end{aligned}$$

Integrating with  $q$ , we find that the first, second, and the third terms in the above equation give terms  $\propto k^0$ ,  $\propto k^1$ , and  $\propto k^0$ , respectively. Taking these terms together, we can find the  $k$  dependence of the magnetic field spectrum as

$$a^4 \frac{k^3}{2\pi^2} S_B(k) \propto k [1 + \mathcal{O}(1/k\eta)]. \quad (4.13)$$

Therefore, in the radiation dominated era ( $\nu = 2$ ), we find  $a^4 k^3 S_B(k)/2\pi^2 \propto k$ , which is confirmed in our numerical calculation. Finally, by reading off the numerical amplitude from the result of our numerical calculation we find the power spectrum of magnetic field on sub-horizon scales as

$$a^4 B^2 \sim \frac{10^{-44}}{(1+z)^3} \frac{1}{N} \left( \frac{v}{10^{-3} m_{pl}} \right)^4 \left( \frac{k}{\text{Mpc}^{-1}} \right)^1 [\text{G}^2] \quad (4.14)$$

Similarly, we find  $a^4 k^3 S_B(k)/2\pi^2 \propto k^{-1}$  in the matter dominated era ( $\nu = 3$ ).

In figure 2, we find that the spectrum shows  $k^3 S_B \propto k$  on small scales (say,  $k \gtrsim 0.1 \text{ Mpc}^{-1}$ ) in the radiation dominated era. At  $z = 2000$  (the red solid line), the spectrum on sub-horizon scales shows the  $k$  dependence between the fully radiation dominated ( $\propto k$ ) and matter dominated ones ( $\propto k^{-1}$ ). On much smaller scales ( $k \gg 1 \text{ Mpc}^{-1}$ ) and in the matter dominated era, we expect that the spectrum of magnetic fields should be proportional to  $k$  because on those scales the source of vector perturbations has already decayed away and the magnetic fields just decay adiabatically after their creation deep in the radiation dominated era. From the fact that the generation mechanism is based on the mass difference between positively charged particles (protons) and negatively charged particles (electrons) and the small velocity slip between these particles, we expect that the spectrum continues up to the horizon scale at the epoch of  $e^\pm$  annihilation  $k \sim 10^{10} \text{ Mpc}^{-1}$  and a cutoff at that scale [20].

### 4.3 Approximation at super-horizon scale

On super-horizon scales and in the radiation dominated era, we can estimate not only the shape of the spectrum but also the amplitude of magnetic fields approximately. On super-horizon scales the power spectrum of magnetic fields is given by

$$a^4(\eta) \frac{k^3}{2\pi^2} S_B(k, \eta) = \frac{k^3}{2\pi^2} \left( \frac{4\sigma_T}{3e} \right)^2 \frac{\mathcal{P}_{\text{ini}}^N}{\pi^2} k^2 \int_0^{1/\eta} dq q^2 \int_{-1}^1 d\mu \left[ \int_0^\eta d\eta' a^2(\eta') \rho_\gamma(\eta') \delta v(k, q, \mu, \eta') \right]^2. \quad (4.15)$$

Substituting eq. (4.2) and eq. (3.7) to eq. (3.5) we get,

$$\sigma(k, q, \mu, \eta) \simeq -\frac{\pi A_\nu}{48} \sqrt{1 - \mu^2} \mu \left( \frac{v}{m_{pl}} \right)^2 \eta^4 \frac{q^2}{k}, \quad (4.16)$$

where we assume  $k \ll q \sim 1/\eta$ . Using the above expression, we can write the velocity slip as

$$\delta v(k, q, \mu, \eta) \approx \frac{\pi A_\nu}{180} R^{-1} \dot{\tau}^{-2} \sqrt{1 - \mu^2} \mu \left( \frac{v}{m_{pl}} \right)^2 \eta^4 q^2 k. \quad (4.17)$$

Substituting eq.(4.17) into eq.(4.15), we obtain

$$a^4(z) \frac{k^3}{2\pi^2} S_B(k, z) \sim \frac{10^{-3}}{(1+z)^9} \frac{1}{N} \left( \frac{v}{m_{pl}} \right)^4 \left( \frac{k}{\text{Mpc}^{-1}} \right)^7 [\text{G}^2], \quad (4.18)$$

in unit of Gauss at redshift  $z \gg z_{\text{eq}} \approx 3300$  [24]. This analytic power is plotted in figure 2 to make a comparison with numerical results.

### 4.4 After recombination

In the above sections, we discussed magnetic field generation in the era when the tight coupling approximation is valid. Here we consider the era after the tight coupling approximation breaks down. In particular, we estimate when the magnetic fields become source-free on super-horizon scales, by considering the time evolution of the source function of magnetic fields  $S(\eta) = \rho_\gamma a^2 \delta v q^{3/2}$ , which satisfies  $B^2 \propto [\int d\eta S]^2$ .

On super-horizon scales ( $k \ll \mathcal{H}$ ), the scalar fields with wavenumbers  $q \sim \mathcal{H}$  have the biggest contribution to the source of vector perturbations and hence the magnetic fields. Thus we can set  $q \sim 1/\eta$  in investigating the behavior of the source. When the tight coupling approximation is valid, i.e.  $z \gg z_{\text{rec}}$ , we can estimate the time evolution of  $\delta v$  as

$$\delta v \propto k^2 \frac{\eta}{\dot{\tau}} \sigma \propto \eta^7, \quad (4.19)$$

from eq. (3.10) and eq. (3.11). Then after recombination, we can estimate  $\delta v \approx v_\gamma$  from the same equations as

$$\delta v \propto k^2 \eta^2 \sigma \propto \eta^4. \quad (4.20)$$

Using these relations, the time evolution of the source term of magnetic fields before and after recombination can be derived as

$$S(\eta) = \rho_\gamma a^2 v_\gamma q^{3/2} \propto \begin{cases} \eta^{3/2} & (\text{before recombination}) \\ \eta^{-3/2} & (\text{after recombination}) \end{cases}. \quad (4.21)$$

Therefore, the evolution of magnetic fields becomes source-free after recombination. In fact, during recombination,  $\delta v$  is considerably enhanced and significant amount of magnetic fields is produced by the end of recombination  $z \gtrsim 300$ . For  $z \lesssim 300$ , the magnetic fields simply decay adiabatically. The spectrum of magnetic fields after recombination is depicted in figure 3.

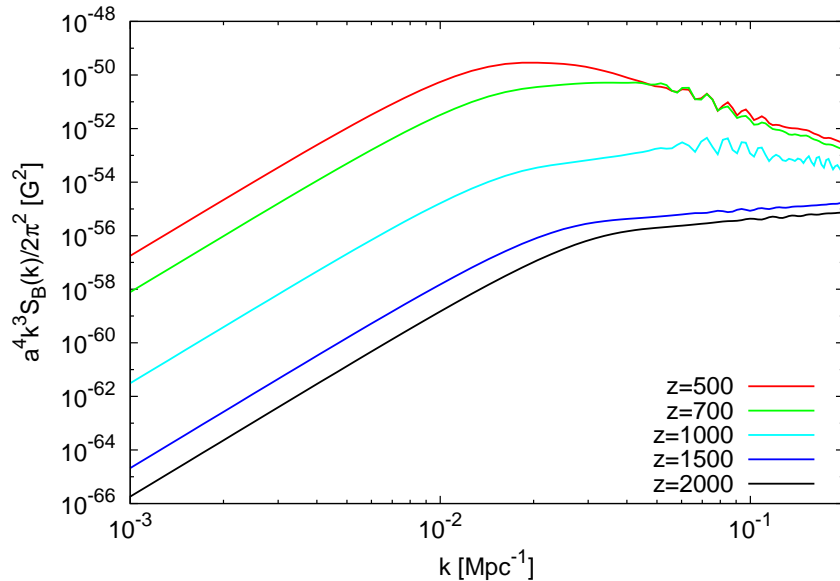


**Figure 3.** Power spectra of magnetic fields at  $z = 2000$  (black solid line), 1500 (green solid line), 1000 (cyan solid line), 700 (green solid line), and 500 (red solid line) from scalar fields in the NLSM. Here we take the NLSM parameters as  $v^4/N = 10^{-12} m_{pl}^4$ . The evolution of the spectrum comes to an end by  $z = 300$ .

## 5 Conclusion

In this paper, we consider magnetic field generation from self-ordering scalar fields that follow the NLSM. We find that to reliably estimate the magnetic fields, one needs to expand the Boltzmann equations up to the third order terms in the tight coupling approximation. This is because the vorticity  $\sigma$  is very large so that  $\mathcal{O}((k/\dot{\tau})v_\gamma) \sim \mathcal{O}((k/\dot{\tau})^3\sigma)$  in the tight coupling era (see figure.1) if the anisotropic stress of the scalar fields eq. (3.6) is an external source. By smoothly connecting the tight coupling solutions to the numerical ones we obtain the full magnetic field spectrum in the radiation dominated era and the matter dominated era, with an analytic interpretation of the results. In so doing, we see that the scalar fields with wavenumber  $q \sim 1/\eta$  are the main source for both super-horizon ( $k\eta \ll 1$ ) and sub-horizon ( $k\eta \gg 1$ ) magnetic fields. By extrapolating our numerical result toward smaller scales analytically, we find  $B \sim 10^{-22} (v/10^{-3} m_{pl})^2 (1+z)^{1/2} (k/\text{Mpc}^{-1})^{1/2} / \sqrt{N}$  Gauss at  $k \gtrsim 1 \text{ Mpc}^{-1}$  and  $z \gtrsim z_{\text{rec}}$ . This might serve as a seed of large scale magnetic fields in the present universe.

## Acknowledgement

This work is supported by Grant-in-Aid for Scientific Research No.25287057 (N.S.) and 24340048 (K.I.). T.S. is supported by the Academy of Finland grant 1263714.

## A Appendix

### A.1 Appendix A : Power spectrum in the NLSM

Let us consider the power spectrum of some variable  $X(\vec{k})$  and  $Y(\vec{k})$  which is generated by scalar fields following the NLSM. At first, let us write  $X(\vec{k})$  using its transfer function  $F_X(q, p)$  and  $F_Y(q, p)$  as

$$X(\vec{k}) = \int \frac{d^3 p}{(2\pi)^3} \frac{d^3 q}{(2\pi)^3} F_X(q, p) \beta_s(\vec{p}) \beta_s(\vec{q}) (2\pi)^3 \delta(\vec{k} - \vec{p} - \vec{q}), \quad (\text{A.1})$$

and a similar expression for  $Y(\vec{k})$ . The (cross) power spectrum of  $X$  and  $Y$  is defined by

$$\langle X(\vec{k}) Y^*(\vec{k}') \rangle \equiv (2\pi)^3 \mathcal{P}_{XY}(k) \delta(\vec{k} - \vec{k}'). \quad (\text{A.2})$$

To calculate the power spectrum, we need to calculate four point correlation function of scalar fields. This is given by

$$\begin{aligned} \langle \beta_a(\vec{q}_1) \beta_a(\vec{p}_1) \beta_b^*(\vec{q}_2) \beta_b^*(\vec{p}_2) \rangle &= \langle \beta_a(\vec{q}_1) \beta_a(\vec{p}_1) \rangle \langle \beta_b^*(\vec{q}_2) \beta_b^*(\vec{p}_2) \rangle \\ &\quad + \langle \beta_a(\vec{q}_1) \beta_b^*(\vec{q}_2) \rangle \langle \beta_a(\vec{p}_1) \beta_b^*(\vec{p}_2) \rangle \\ &\quad + \langle \beta_a(\vec{q}_1) \beta_b^*(\vec{p}_2) \rangle \langle \beta_a(\vec{p}_1) \beta_b^*(\vec{q}_2) \rangle \\ &= (6\pi^2)^2 (2\pi)^3 \delta(\vec{p}_1 + \vec{q}_1) (2\pi)^3 \delta(\vec{p}_2 + \vec{q}_2) \\ &\quad + \frac{(6\pi^2)^2}{N} (2\pi)^3 \delta(\vec{q}_1 - \vec{q}_2) (2\pi)^3 \delta(\vec{p}_1 - \vec{p}_2) \\ &\quad + \frac{(6\pi^2)^2}{N} (2\pi)^3 \delta(\vec{q}_1 - \vec{p}_2) (2\pi)^3 \delta(\vec{p}_1 - \vec{q}_2). \end{aligned} \quad (\text{A.3})$$

Here,  $\frac{(6\pi^2)^2}{N} = \mathcal{P}_{\text{ini}}^N$  is the initial power spectrum of the scalar fields. Substituting eq. (A.3) to eqs. (A.1) and (A.2), and using  $F(q, p) = F(p, q)$ , we calculate the cross correlation as

$$\begin{aligned} \langle X(\vec{k}) Y^*(\vec{k}') \rangle &= \int \frac{d^3 q_1}{(2\pi)^3} \frac{d^3 p_1}{(2\pi)^3} \frac{d^3 q_2}{(2\pi)^3} \frac{d^3 p_2}{(2\pi)^3} F_X(q_1, p_1) F_Y^*(q_2, p_2) \langle \beta_a(\vec{q}_1) \beta_a(\vec{p}_1) \beta_b^*(\vec{q}_2) \beta_b^*(\vec{p}_2) \rangle \\ &\quad \times (2\pi)^3 \delta(\vec{k} - \vec{p}_1 - \vec{q}_1) (2\pi)^3 \delta(\vec{k}' - \vec{p}_2 - \vec{q}_2) \\ &= \int \frac{d^3 q_1}{(2\pi)^3} \frac{d^3 p_1}{(2\pi)^3} \frac{d^3 q_2}{(2\pi)^3} \frac{d^3 p_2}{(2\pi)^3} F_X(q_1, p_1) F_Y^*(q_2, p_2) \\ &\quad \left[ \frac{(6\pi^2)^2}{N} (2\pi)^3 \delta(\vec{q}_1 - \vec{q}_2) (2\pi)^3 \delta(\vec{p}_1 - \vec{p}_2) + \frac{(6\pi^2)^2}{N} (2\pi)^3 \delta(\vec{q}_1 - \vec{p}_2) (2\pi)^3 \delta(\vec{p}_1 - \vec{q}_2) \right] \\ &\quad \times (2\pi)^3 \delta(\vec{k} - \vec{p}_1 - \vec{q}_1) (2\pi)^3 \delta(\vec{k}' - \vec{p}_2 - \vec{q}_2) \\ &= \mathcal{P}_{\text{ini}}^N (2\pi)^3 \delta(\vec{k} - \vec{k}') \\ &\quad \times \int \frac{d^3 q}{(2\pi)^3} \left[ F_X(q, |\vec{k} - \vec{q}|) F_Y^*(q, |\vec{k} - \vec{q}|) + F_X(|\vec{k} - \vec{q}|, q) F_Y^*(q, |\vec{k} - \vec{q}|) \right] \\ &= 2\mathcal{P}_{\text{ini}}^N (2\pi)^3 \delta(\vec{k} - \vec{k}') \int \frac{d^3 q}{(2\pi)^3} F_X(q, |\vec{k} - \vec{q}|) F_Y^*(q, |\vec{k} - \vec{q}|). \end{aligned} \quad (\text{A.4})$$

Therefore the power spectrum  $\mathcal{P}_{XY}$  is read off as

$$\begin{aligned} \mathcal{P}_{XY}(k) &= 2\mathcal{P}_{\text{ini}}^N \int \frac{d^3 q}{(2\pi)^3} F_X(q, |\vec{k} - \vec{q}|) F_Y^*(q, |\vec{k} - \vec{q}|) \\ &= \frac{\mathcal{P}_{\text{ini}}^N}{2\pi^2} \int dq q^2 \int d\mu F_X(q, |\vec{k} - \vec{q}|) F_Y^*(q, |\vec{k} - \vec{q}|), \end{aligned} \quad (\text{A.5})$$

where  $\mu = \hat{k} \cdot \hat{q}$ .

## References

- [1] R. Durrer, *Gauge invariant cosmological perturbation theory: A General study and its application to the texture scenario of structure formation*, Fund.Cosmic Phys. **15** (1994) 209, [[astro-ph/9311041](#)].
- [2] R. Durrer, A. Gangui, and M. Sakellariadou, *Doppler peaks: A Fingerprint of topological defects*, Phys.Rev.Lett. **76** (1996) 579–582, [[astro-ph/9507035](#)].
- [3] R. Durrer, M. Kunz, and A. Melchiorri, *Cosmic microwave background anisotropies from scaling seeds: Global defect models*, Phys.Rev. **D59** (1999) 123005, [[astro-ph/9811174](#)].
- [4] U.-L. Pen, U. Seljak, and N. Turok, *Power spectra in global defect theories of cosmic structure formation*, Phys.Rev.Lett. **79** (1997) 1611–1614, [[astro-ph/9704165](#)].
- [5] E. Fenu, D. G. Figueroa, R. Durrer, and J. García-Bellido, *Gravitational waves from self-ordering scalar fields*, jcap **10** (Oct., 2009) 5, [[arXiv:0908.0425](#)].
- [6] J.-F. Dufaux, D. G. Figueroa, and J. García-Bellido, *Gravitational waves from Abelian gauge fields and cosmic strings at preheating*, Phys. Rev. D **82** (Oct., 2010) 083518, [[arXiv:1006.0217](#)].
- [7] K. Jones-Smith, L. M. Krauss, and H. Mathur, *A Nearly Scale Invariant Spectrum of Gravitational Radiation from Global Phase Transitions*, Phys.Rev.Lett. **100** (2008) 131302, [[arXiv:0712.0778](#)].
- [8] J. T. Giblin, Jr., L. R. Price, X. Siemens, and B. Vlcek, *Gravitational waves from global second order phase transitions*, jcap **11** (Nov., 2012) 6, [[arXiv:1111.4014](#)].
- [9] D. G. Figueroa, M. Hindmarsh, and J. Urrestilla, *Exact Scale-Invariant Background of Gravitational Waves from Cosmic Defects*, Physical Review Letters **110** (Mar., 2013) 101302, [[arXiv:1212.5458](#)].
- [10] C. Hill, D. Schramm, and T. Walker, *Ultra-high-energy cosmic rays from superconducting cosmic strings*, Phys. Rev. D **36** (Aug, 1987) 1007–1016.
- [11] A. J. Gill and T. W. B. Kibble, *Cosmic rays from cosmic strings*, prd **50** (Sept., 1994) 3660–3665, [[hep-ph/9403395](#)].
- [12] R. Durrer, M. Kunz, and A. Melchiorri, *Cosmic structure formation with topological defects*, Phys. Rep. **364** (June, 2002) 1–81, [[astro-ph/0110348](#)].
- [13] **Planck Collaboration** Collaboration, P. Ade et al., *Planck 2013 results. XXV. Searches for cosmic strings and other topological defects*, [arXiv:1303.5085](#).
- [14] J. Urrestilla, N. Bevis, M. Hindmarsh, and M. Kunz, *Cosmic string parameter constraints and model analysis using small scale Cosmic Microwave Background data*, JCAP **1112** (2011) 021, [[arXiv:1108.2730](#)].
- [15] **BICEP2 Collaboration** Collaboration, P. Ade et al., *Detection of B-Mode Polarization at Degree Angular Scales by BICEP2*, Phys.Rev.Lett. **112** (2014) 241101, [[arXiv:1403.3985](#)].
- [16] L. M. Krauss, *Gravitational waves from global phase transitions*, Phys.Lett. **B284** (1992) 229–233.
- [17] E. Fenu, D. G. Figueroa, R. Durrer, J. Garcia-Bellido, and M. Kunz, *Cosmic Microwave Background temperature and polarization anisotropies from the large- $N$  limit of global defects*, [arXiv:1311.3225](#).
- [18] R. Durrer, D. G. Figueroa, and M. Kunz, *Can Self-Ordering Scalar Fields explain the BICEP2 B-mode signal?*, JCAP **1408** (2014) 029, [[arXiv:1404.3855](#)].



- [19] J. Lizarraga, J. Urrestilla, D. Daverio, M. Hindmarsh, M. Kunz, et al., *Constraining topological defects with temperature and polarization anisotropies*, [arXiv:1408.4126](#).
- [20] K. Ichiki, K. Takahashi, and N. Sugiyama, *Constraint on the primordial vector mode and its magnetic field generation from seven-year wilkinson microwave anisotropy probe observations*, Phys. Rev. D **85** (Feb, 2012) 043009.
- [21] A. Neronov and I. Vovk, *Evidence for Strong Extragalactic Magnetic Fields from Fermi Observations of TeV Blazars*, Science **328** (Apr., 2010) 73–, [[arXiv:1006.3504](#)].
- [22] K. L. Pandey and S. K. Sethi, *Probing Primordial Magnetic Fields Using Ly $\alpha$  Clouds*, apj **762** (Jan., 2013) 15, [[arXiv:1210.3298](#)].
- [23] M. L. Bernet, F. Miniati, S. J. Lilly, P. P. Kronberg, and M. Dessauges-Zavadsky, *Strong magnetic fields in normal galaxies at high redshifts*, Nature **454** (2008) 302–304, [[arXiv:0807.3347](#)].
- [24] **Planck Collaboration** Collaboration, P. Ade et al., *Planck 2013 results. XVI. Cosmological parameters*, Astron.Astrophys. (2014) [[arXiv:1303.5076](#)].
- [25] C.-P. Ma and E. Bertschinger, *Cosmological perturbation theory in the synchronous and conformal Newtonian gauges*, Astrophys.J. **455** (1995) 7–25, [[astro-ph/9506072](#)].
- [26] A. Lewis, *Observable primordial vector modes*, prd **70** (Aug., 2004) 043518, [[astro-ph/0403583](#)].
- [27] K. Ichiki, K. Takahashi, N. Sugiyama, H. Hanayama, and H. Ohno, *Magnetic Field Spectrum at Cosmological Recombination*, ArXiv Astrophysics e-prints (Jan., 2007) [[astro-ph/0701329](#)].
- [28] S. Saga, M. Shiraishi, K. Ichiki, and N. Sugiyama, *Generation of magnetic fields in Einstein-Aether gravity*, Phys.Rev. **D87** (2013), no. 10 104025, [[arXiv:1302.4189](#)].